Wetting and Molecular Dynamics Simulations of Simple Liquids

J. De Coninck and T.D. Blake

Center for Research in Molecular Modeling, University of Mons-Hainaut, 7000 Mons, Belgium; email: joel.de.coninck@crmm.umh.ac.be, terrydblake@btinternet.com

Annu. Rev. Mater. Res. 2008. 38:15.1–15.22

The *Annual Review of Materials Research* is online at matsci.annualreviews.org

This article's doi:
10.1146/annurev.matsci.38.060407.130339

1531-7331/08/0804-0001$20.00

Key Words

wetting dynamics, molecular-kinetic theory, solid-liquid interactions, spreading

Abstract

Large-scale molecular dynamics simulations are increasingly applied to the study of wetting dynamics. They have the advantage of being able not only to model the macroscopic world with reasonable accuracy, but also to reveal details at the microscopic level. Here we review the principles of modeling, using molecular dynamics, and comment on the specific methods used in our laboratory in comparison with others. By way of example, we explain how we extract physical parameters from simulations of partially wetting liquids on homogeneous substrates in a variety of geometries. We then show how the results have been applied to build our understanding of the underlying mechanisms.

1. INTRODUCTION

Contact line: the mathematical line at which solid-liquid, liquid-vapor, and solid-vapor interfaces meet

TPZ: three-phase zone

Dissipation channels: when a sessile drop spreads on top of a solid surface, its shape changes versus time, leading to the dissipation of energy. Current theories describing this process differ in terms of the principal dissipation channels considered, i.e., viscous dissipation in the hydrodynamic theories and contact-line friction in the molecular-kinetic theory

MKT: molecular-kinetic theory

MD: molecular dynamics

To explain the dynamic wetting behavior of liquids on solids, it is necessary to understand the processes that occur in the immediate vicinity of the moving three-phase contact line. These processes are dissipative and are associated, not only with the fluid flow within this region, but also with the creation (in the case of wetting) of new solid-liquid interface. A key region, therefore, is the three-phase zone (TPZ), i.e., that region of small but finite dimensions where the liquid-vapor, solid-liquid, and solid-vapor interfaces meet. Here the processes act on the microscopic scale and so will depend strongly on the molecular properties of the particular liquids and solids involved.

Several theories of dynamic wetting have been formulated to account for the observed macroscopic behavior and have been recently reviewed (1). Overall, we may expect that some general quantifiable behavior exists and that the particularities of the system can be captured by specific parameters. The various hydrodynamic models of wetting (e.g., References 2–6) and the complementary molecular-kinetic theory (MKT) (7–12) have yielded significant advances in this direction. Yet, one faces a question: How do we verify if these models are correct, especially at the microscopic level of the TPZ? Although experimental methods evolve very rapidly, it is still hardly possible to get a clear picture. Another approach is required. One such line of attack is to use computer simulations: Starting from assumptions about the individual molecules and the interactions between them, computer simulations may reveal collective results that in turn can be used to reveal the underlying mechanism of wetting.

With the development of powerful computers, simulation techniques have been increasingly used in the scientific world. From the first Monte Carlo simulations of liquids by Metropolis et al. (13) in 1953, the field of computer simulations developed rapidly. In 1957, Alder & Wainwright (14) used a molecular dynamics (MD) simulation to describe the solution of the classical equations of motion (Newton's equations) for a set of molecules. In 1964, Rahman (15) introduced Lennard-Jones potentials to describe molecular interactions. Saville (16) in 1977 presented one of the first convincing MD simulations of wetting. Since then, the capability of MD simulation has closely mirrored the exponential growth of computer power. Now we are at the point at which we can simulate protein molecules in all their complexity or, alternatively, the collective behavior of thousands of simpler molecules.

Computer simulations are very useful for solving problems in the field of statistical mechanics, in which often no exact solutions exist and in which it is necessary to verify the various approximations on the basis of physical arguments. The results of simulations can then be compared with experiment, which allows one to test the applied model and access the parameters used. Monte Carlo and MD simulations have been used extensively, especially for the study of the local structure of liquids (17).

Progress in applying simulations to the study of wetting dynamics has been made along a number of fronts. For example, Monte Carlo calculations of the dynamics of spreading of completely wetting liquids, through the use of Kawasaki dynamics with a local conservation law for the number of molecules (18), have produced results in general agreement with experiment. However, the application of Monte Carlo simulations to nonequilibrium dynamics is not really justified, and the use of more rigorous MD simulations has enabled us to unravel the mechanisms of layered spreading in much greater detail (19–21).

A second thread of research has concerned MD studies of partially wetting two-phase systems confined between parallel walls and undergoing either Poiseuille (22, 23) or Couette (24, 25) flow. These systems appeared to exhibit macroscopic (continuum) behavior at the system level, but it was revealed that the dissipation mechanisms close to the moving contact line are rather

complex. Although the simulations were comparatively small (~5000 atoms), reliable results could be obtained for large angles as the systems were analyzed under steady-state conditions.

Since these pioneering studies, several groups have carried out larger-scale simulations of systems that mimic those of many other classical wetting experiments. These include drops (26–28) and cylinders (29) spreading on flat surfaces, liquid rise in capillaries (30) and around fibers (31), and the forced wetting of flat surfaces and fibers (32, 33). Research has also extended to more complex systems such as liquids spreading on heterogeneous (34, 35), chemically patterned (36), or porous (37) surfaces; spreading binary droplets (29) and monolayers (38); liquid penetration into carbon nanotubes (39); and the spreading of liquid metals on ceramic and metal substrates (40–42). In addition, simulations of dewetting have been reported quite recently (43). Taken together, the studies have confirmed that the general behavior of the simulated systems and that of key macroscopic variables, such as the dynamic contact angle, closely reflect what is observed in real physical experiments. Moreover, it has been possible to test existing theoretical descriptions and in some cases to verify these at the molecular level.

Dynamic contact angle: the contact angle associated with a moving contact line

Contact angle: the angle between normals to the fluid-fluid interface and the solid surface at the contact line. For a solid-liquid-vapor system, the angle is usually measured through the liquid

In this chapter, we show how large-scale MD simulations can indeed help us to investigate wetting mechanisms and validate models. If the system contains enough liquid molecules, we can measure all the macroscopic parameters, such as the density, surface tension, viscosity, flow, and dynamic contact angle. At the same time, we can also measure every molecular parameter that is considered important for wetting behavior. Crucially, MD simulations enable us to change individual parameters separately in a way that would not be possible in an experiment. For example, we can systematically vary the solid-liquid interaction and follow its direct influence on wetting. In experiments with real materials, changing the solid-liquid interaction would necessitate changes in solid-solid or liquid-liquid interactions and cause changes in dependent quantities such as the liquid viscosity and surface tension.

Thus, MD gives us a powerful tool to study the influence of individual parameters quite independently of any others and, in combination with theory and experiment, can lead to a better understanding of the physics of wetting. On the negative side, practical simulations are still restricted to physically small systems of the order of a few tens of nanometers and short times of the order of a few nanoseconds. The simulations are therefore subject to noticeable thermal and statistical fluctuations. This limitation is, however, just a matter of time and computer power and is being eroded continuously.

In what follows, we first explain the principles of modeling using MD. Next, we expand more on the specific methods used in our simulations in comparison with others. By way of example, we explain how we extract physical parameters from simulations of partial wetting systems on homogeneous substrates carried out in this laboratory. We then show how the results have been applied to build our understanding of the underlying mechanisms. In the last section, we summarize our conclusions and point the way forward.

2. BASIC METHODS

With the use of the most powerful computers and the latest mathematical techniques, we are now able to simulate the dynamic behavior of 10^6 atoms. This number is very small compared with the number of atoms in a typical experimental system (say, 10^{23}). Nevertheless, in addition to the microscopic details, useful macroscopic characteristics can be deduced from the simulations. For systems containing such a large number of atoms, the interactions are necessarily restricted to the short-range. Moreover, only phenomena that occur over sufficiently short times (~10^{-8} s) can be studied. Although this is a limitation that must be accommodated, it does not prevent us from simulating phenomena that are representative of the real world.

All outcomes within a MD simulation are completely deterministic. All molecules, or atoms for that matter, obey Newton's equations, which are reversible in time. This does not mean that the processes studied at the system level are reversible. Apart from computational rounding errors, which prevent exact time reversal, the modeled processes are dissipative, and the heat generated must be managed to simulate isothermal behavior. The principal interactions are usually modeled with Lennard-Jones potentials (17). At time t, the positions ($\mathbf{r}_i$), the velocities ($\mathbf{v}_i$), and the accelerations ($\mathbf{a}_i$) of all n atoms are calculated from their values at time ($t - \Delta t$). To make the simulations as general as possible, all values of the physical quantities within a simulation are expressed in terms of dimensionless parameters. Only three principal parameters need be specified. The units of length and energy are given, respectively, by the parameters σ and ε, which appear in the Lennard-Jones equations. The unit of mass is typically chosen as the mass of a carbon atom or an argon atom.

In general, the interatomic potential $V_{ij}(r)$ between atoms i and j at distance r is chosen a priori, and the related forces are simply calculated as the derivative in space. For a given time, the accelerations are then calculated as $\mathbf{a}_i = \mathbf{F}_i/m_i$. From the acceleration, the velocity and the positions are determined by integrating over time. To perform this calculation, small discrete time steps Δt have to be imposed. The best value for Δt is a compromise. On the one hand, we would like Δt to be as large as possible, to increase the efficiency of the simulation. On the other hand, Δt should be much smaller than the average time between two molecular collisions (interactions).

To solve the resulting differential equations, we used the predictor-corrector algorithm (44). Only the initial values for the positions and the velocities of the atoms are specified a priori. In MD, it is very common to apply periodic boundary conditions to increase artificially the size of the system. However, in most of our simulations (e.g., a liquid drop on a solid substrate, with almost no gas phase), we do not use this approach to extend the liquid to avoid interactions between the liquid and its periodic image.

The methods outlined above allow us to study the collective behavior of large sets of particles in situations in which no analytical description is possible. The next step is to apply these methods to specific models.

3. MODELS

The basic components used in the simulations of wetting are a pool of liquid (L) and a flat solid substrate (S). The liquid molecules are typically n-atom chains, with n between 2 and 64, but chains of up to 100 units have been studied (29, 36). By considering chains rather than single atoms, we increase the viscosity of the liquid to more realistic values and considerably reduce evaporation into the surrounding vacuum. Depending on the objectives, different models can be considered, ranging from realistic simulations dealing with complex interactions mimicking key steps in a larger experiment, to more qualitative simulations dealing with simplistic interactions aimed at discriminating the general details of the mechanisms controlling wetting.

The molecules of the liquid interact both with each other and with the atoms of the solid; it is the balance of these interactions that determines the equilibrium wetting state. For simplicity, we assume that the interaction is via a pair-wise Lennard-Jones potential:

$$U_{ab} = 4\varepsilon_{ab}(C_{ab}(\sigma_{ab}/r_{ij})^{12} - D_{ab}(\sigma_{ab}/r_{ij})^{6}), \qquad 1.$$

where, for a given pair of atoms a and b, the coefficients ε_{ab} and σ_{ab} are related in the usual way to the depth of the potential well and the effective molecular diameter, respectively, and r_{ij} is the distance of separation (17). It is expedient to use the same values of $\varepsilon_{ab} = 33.33°\mathrm{K}$ (4.6×10^{-22} J)

and $\sigma_{ab} = 3.5$ Å for the different types of interaction: *L*-*L*, *S*-*S*, and *L*-*S*. The choice is arbitrary but allows us to set the values systematically (30) and ensure that the *L*-*S* interactions are consistent with the Lorentz-Berthelot rule: $\sigma_{ab} = 0.5(\sigma_{aa} + \sigma_{bb})$, $\varepsilon_{ab} = (\varepsilon_{aa}\varepsilon_{bb})^{0.5}$.

The coefficients C_{ab} and D_{ab} that appear in Equation 1 permit us to selectively increase or decrease the repulsive (C_{ab}) or attractive (D_{ab}) parts of the potential to specify the coupling between different types of atoms. This allows us to study the influence of the wettability of the solid surface with respect to the liquid.

The range of the Lennard-Jones potential is theoretically infinite. Hence, in principle, one should consider the interactions between all possible pairs of atoms in the system. Fortunately, however, the potential decreases very steeply with interatomic distance. Therefore, to a good approximation (19, 20), we can truncate the potential at a relatively small cut-off radius, usually 2.5σ, which substantially reduces the number of computations. The Lennard-Jones potentials provide the essential framework for the molecular interactions in the system, but to improve realism it is necessary to add some additional elements.

To maintain a constant distance between any two adjacent atoms within a given liquid molecule, we incorporate a confining potential between nearest neighbors i and j: $V_{conf}(r_{ij}) = Ar_{ij}^6$. The power 6 is chosen for computational convenience (45). The constant A is derived from the Lennard-Jones parameters and is defined as $A = \varepsilon_{LL}/(\sigma_{LL})^6$. V_{conf} and ε_{LL} are expressed in the same units of energy, and r_{ij} and σ_{LL} are expressed in the same units of distance.

The solid substrate in our simulations is typically a square planar lattice of three atomic layers with periodic boundary conditions. Three layers are sufficient if one bears in mind the spherical cut-off for the Lennard-Jones potential. Each solid atom is placed at a lattice node 3.93 Å from its four nearest neighbors, corresponding to $2^{1/6}\,\sigma_{SS}$. The atoms of the solid vibrate thermally around their initial equilibrium position according to a harmonic potential of the form $V_H = B(r_i - r_i^0)^2$, where r_i is the instantaneous position of a solid atom and r_i^0 its equilibrium position (38, 45). The constant B is again derived from the Lennard-Jones parameters and is defined as $B = 2.5(\varepsilon_{SS}(\sigma_{SS})^2)$. Although this specification is very simple, we believe that it provides a realistic model of a solid surface.

Substrates with face-centered-cubic or hexagonal lattices have also been employed in dynamic wetting (28, 33) and related (e.g., 46–48) studies of liquid mobility (slip) at solid surfaces. In Reference 47 the solid atoms are positioned at fixed lattice nodes, and heat exchange is managed through the use of a Nosé-Hoover thermostat (49, 50). Other simulations (28, 29, 36) employ nonatomistic, flat solids. However, although these strategies yield computational economies and probably have no significant effect on the equilibrium properties of the system, the specific choices could affect the details of the dissipation mechanism controlling dynamic wetting. Although there are several techniques to control the heat exchange between the substrate and the liquid (28), as far as we are aware no systematic study of the implication of such choices has been undertaken. In modeling dynamic processes such as wetting and slip, the transfer of momentum between the solid and the liquid is a critical factor. It therefore seems important to model this as accurately as possible to capture the correct molecular mechanism. That a simulation exhibits realistic macroscopic behavior (contact angle versus velocity or droplet radius versus time, for example) is not sufficient to guarantee that the molecular mechanism is also realistic.

To define a timescale for our simulations, it is necessary to assign masses to the atoms. For all the atoms (*L* and *S*), we set $m_L = m_S = 12$ g mol^{-1}, i.e., the molar mass of carbon. Once again, the choice is arbitrary but does not affect the results qualitatively and allows comparison with other relevant studies. The time step between computational iterations is classically fixed to 0.005 ps, and all the simulations are carried out at a fixed temperature T.

4. MEASUREMENTS

We here illustrate the procedure with reference to studies of spreading liquid drops. With appropriate modifications the methods can be applied to other configurations. In each simulation, a set of liquid molecules and a set of solid atoms are initially placed far from each other, so that they can equilibrate independently. The shape of the liquid ensemble changes rapidly from its initial form (cubic, for instance) to a sphere. The solid atoms remain confined to their lattice. During this period, the temperatures of both the liquid and the solid are held constant by renormalizing the speeds of the constituent atoms to maintain their kinetic energy constant. Once the liquid has achieved its equilibrium configuration, it is brought to a distance from the wall, where the interactions between the liquid and the solid start to develop [2.5 in reduced units (r.u.) according to the model described previously]. From that moment on, the system is free to evolve, with just the temperature of the wall held constant to avoid heating the system owing to the dissipation processes occurring during wetting.

As the liquid meniscus spreads on top of the solid, the meniscus's shape changes as it relaxes toward its new equilibrium configuration. **Figure 1** shows a snapshot of the side view of such a drop. To describe the dynamics, we need to record the shape versus time t. To do this, we have to locate the edge of the meniscus. To characterize our observations, we can then study either the contact angle that the meniscus makes with the solid or the radius of the contact area between the liquid and the solid. The initial step is to define these variables within the simulation. The details of the procedure may vary with geometry, but the approach remains essentially the same.

We first measure, layer by layer, the radial density profile of the liquid atoms within the drop. We then locate the extremity of the layer from the radial distribution, using an appropriate cut-off value (0.4, 0.5, or 0.6). More complex criteria may be used to locate the interface, e.g., sigmoidal functions, but these lead essentially to the same results. Because gravity is absent and viscous stresses are small (low capillary number), we can fit a circular profile through the cut-off points of all the layers. This defines the meniscus. It is necessary to check that the result does not depend significantly on the thickness of the layers considered or on the cut-off density. Overall, the aim is to mimic a real experiment. To this end, we omit the first few (less than ten) layers of liquid atoms

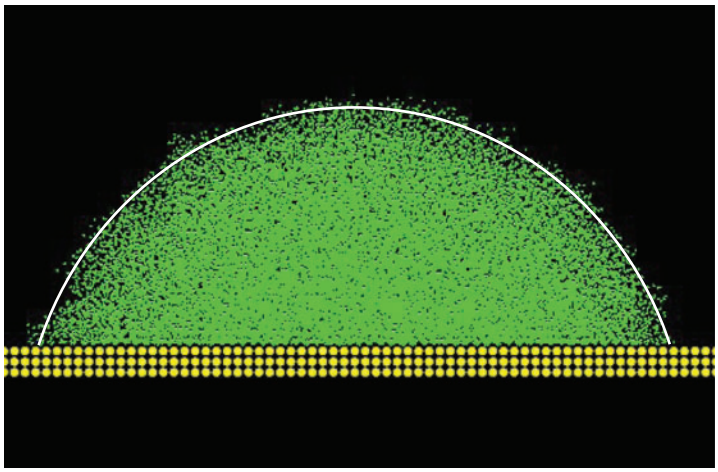

Figure 1

Snapshot of a spreading drop. The white line shows the best circular fit to the profile, excluding the first ten layers near the wall.

in contact with the wall. Here, we may expect rather strong entropic effects (surface-induced layering) and the appearance of a "foot." As a result, it is also necessary to confirm that the results do not depend significantly on the number of layers in contact with the wall that are neglected. From the circular fits, elementary trigonometry gives the contact angle versus the time.

These considerations bring us back to the definition of the contact angle. In the derivation by Gibbs, the contact angle is introduced through the use of thermodynamics and, in consequence, macroscopic arguments. On a macroscopic scale, the short-range deviation of the profile from a circle near the wall is negligible and is never considered. From an experimental point of view, the profile of a macroscopic drop without external forces is circular, and the contact angle is the angle tangent to this profile, measured at the point where the liquid meets the solid substrate. Deviations up to a few nanometers away from the solid are not considered. We therefore assume that the contact angle in our simulations may be determined from the extrapolated circle through the profile, excluding the region that is influenced by the solid.

The dynamic contact angle can be measured with exactly the same procedure. Experience shows that the perturbed region near the wall is larger during dynamic wetting than at equilibrium but is still confined to within the first ten layers of liquid. By analyzing drops of different sizes (100,480, 25,600, 14,400, and 6400 atoms), we have determined that the thickness of the perturbed region is independent of the size of the drop. This confirms that the perturbation is a localized phenomenon that should not be taken into account in calculating the dynamic contact angle. In **Figure 2** we show an example of the complete relaxation of the contact angle from close to 180° to its equilibrium value at long times. The relaxation curve closely resembles those found experimentally (51).

Upon varying the solid-liquid interactions, we expect to see changes in the equilibrium contact angle. Indeed, to fulfill Young's equation, where only the solid-liquid interfacial tension is dependent on the solid-liquid interactions, the equilibrium contact angle has to change. In **Figure 3**, the results of simulations with different solid-liquid interactions are given for a spreading drop containing 25,600 atoms. As expected, the relaxation curves tend to progressively lower values of the equilibrium contact angle θ^0 as the interaction is increased.

Complementary to these results, we can record the positions of the molecules within the drop at every time step and so analyze the flow. This can help us to understand the convection processes

Young's equation: the necessary mechanical condition for thermodynamic equilibrium for systems containing three-phase contact lines: $\gamma_{S2} - \gamma_{S1} = \gamma_{12} \cos\theta^0$, where fluid 1 is a liquid through which θ^0 is measured and fluid 2 is a second immiscible liquid or a gas

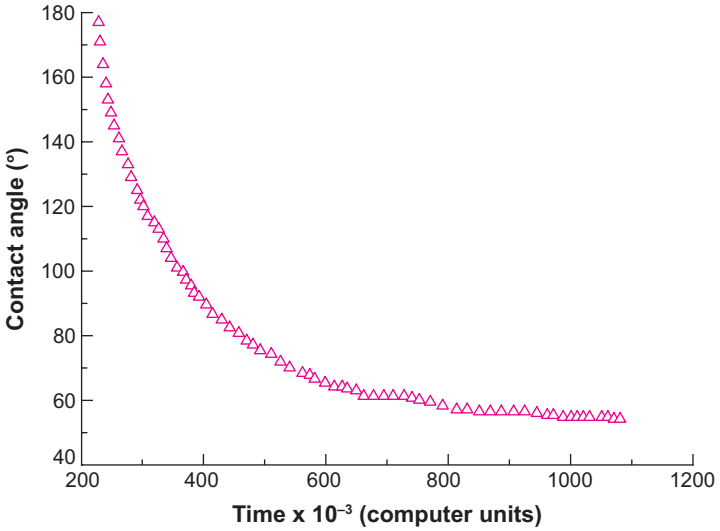

Figure 2

Contact-angle relaxation for a drop consisting of 100,480 liquid atoms, with $C_{SL} = D_{SL} = 0.5$.

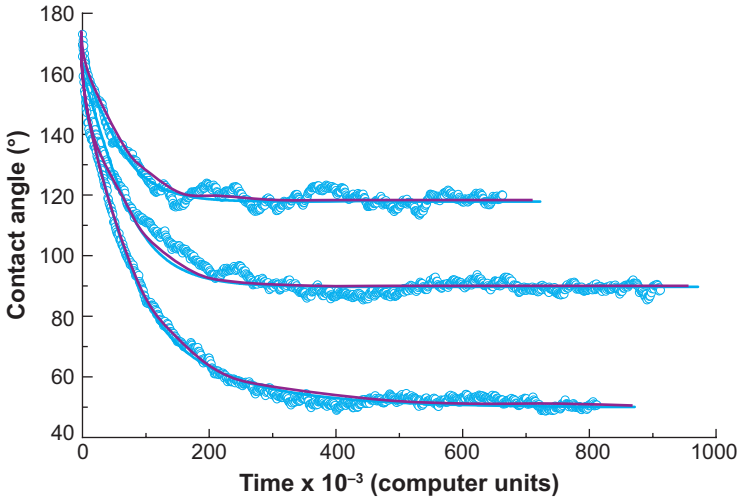

Figure 3

Dependence of contact-angle relaxation on the solid-liquid interaction (25). From top to bottom $C_{SL} = D_{SL} =$ 0.3, 0.4, and 0.5, yielding equilibrium contact angles of $\theta^0 =$ 119°, 88°, and 51°, respectively. The solid lines are fits obtained by the use of the linear form of the MKT (see text).

within the drop. The techniques are based on macroscopic methods and therefore provide a description closely related to hydrodynamics. We begin by subdividing the meniscus into small boxes or "bins." The size of the bins is constrained by the need to maximize the number of bins while ensuring that every bin contains enough atoms to give statistically reproducible results. For every bin, we compute the center of mass of the atoms that are part of that bin. A short time later (typically 10,000 computer time steps), we determine the net displacement of the center of mass. This allows us to measure the velocity field of the drop in some coarse-grained sense. If one assumes that the density in the drop is uniform, the velocity field could be considered as lines of flux (streamlines). In **Figure 4**, velocity fields are shown at intermediate times for a spreading drop of 100,480 atoms with $C_{SL} = D_{SL} = 0.5$. The equilibrium contact angle for this drop is 51°. The instantaneous dynamic contact angle is close to 90°. Away from the solid wall, the velocity field is vertical downward; close to the wall, it is horizontal; and at intermediate height, the direction of the field shifts between the two. In the middle of the drop, the flow is relatively stagnant. Along

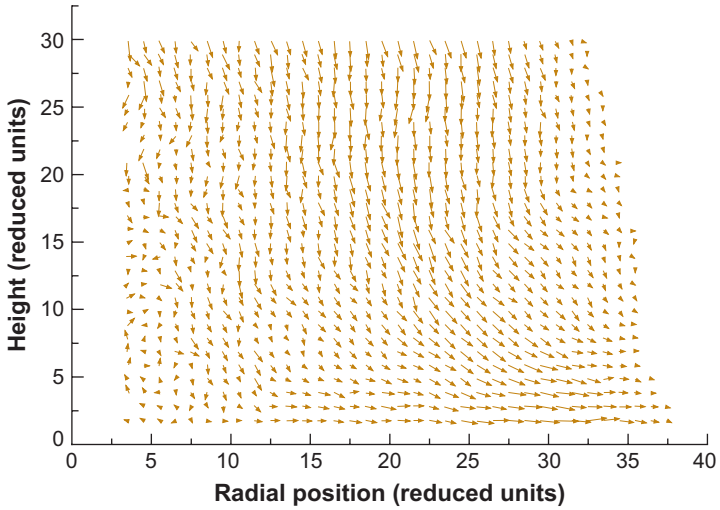

Figure 4

Velocity field of a drop during spreading in the reference frame of the solid (26). The upper part of the drop is not shown. The solid is at $z = 0.55$. The vapor phase is to the right.

the solid, there seems to be a gradient in velocity, approximately zero in the middle of the drop and with the maximum close to the contact line. Along the liquid-vapor interface, the velocities are very small, but just inside the interface a ribbon of flow can be detected.

Similar analysis has been carried out for spreading cylinders (29), wetting of flat surfaces (32) and fibers (31, 33), and capillary penetration (52), revealing variations in flow that reflect the geometry and kinematics of the system in what appears to be a realistic manner. Other quantities such as the surface tension γ or the viscosity η can also be measured by standard techniques, which can be found elsewhere (52a).

5. RESULTS

5.1. Spontaneous Spreading

Through the use of the techniques outlined above, spontaneous spreading of long-chain liquids has been studied for different types of substrates, including flat surfaces, fibers, and a single pore (imbibition). Here we briefly review some of our results and compare them with theory.

5.1.1. Spreading drops on flat substrates. For the contact-angle-relaxation results shown in **Figure 3**, the solid-liquid interaction coefficients $C_{SL} = D_{SL}$ were set at 0.3, 0.4, and 0.5. The resulting equilibrium contact angles were $\theta^0 = 119°$, 88°, and 51°, respectively, i.e., all in the partial wetting regime. Because of this and because over much of the relaxation range the system is not too far from equilibrium, it is reasonable to fit the data, making use of the linear approximation of the MKT to describe the relationship between the dynamic contact angle θ and the contact-line speed v (1):

$$v = \gamma(\cos\theta^0 - \cos\theta)/\zeta^0, \qquad 2.$$

where ζ^0 is the coefficient of contact-line friction arising from dissipation within the TPZ. This coefficient is related to the frequency of molecular displacements at equilibrium K^0 and the length of each displacement λ of the atoms in that region: $\zeta^0 = k_B T/K^0\lambda^3$, where k_B is the Boltzmann constant. Reference 25 provides details of the fitting procedure, assuming a constant volume drop. The results of the fits are depicted by the solid lines in **Figure 3**. Evidently, this simple model is able to account for the data rather well. The resulting values of ζ^0 are listed in **Table 1** and show that the contact-line friction is an increasing function of *S-L* interaction, i.e., decreasing θ^0, as discussed by Blake & De Coninck (11).

By analyzing the displacements in the first layer of liquid atoms adjacent to the solid, we found that λ was 0.8 r.u. perpendicular to the solid and ~1.0 r.u. along the solid for all three interactions. In addition, we established that for the system studied perpendicular displacements were significantly less frequent than those along the solid and were therefore the rate-determining step in contact-line movement (see Subsection 5.3 for details). With λ fixed at 0.8 r.u., we were

Table 1 Values for ζ^0 and K^0 obtained by fitting the data in Figure 3, using the linear approximation of the MKT

Solid-liquid interaction $C_{SL} = D_{SL}$ (r.u.)	θ^0 (°)	ζ^0 (fit) (r.u.)	K^0 (fit) (r.u.)
0.3	119	4.0	0.235
0.4	88	9.3	0.101
0.5	51	10.2	0.093

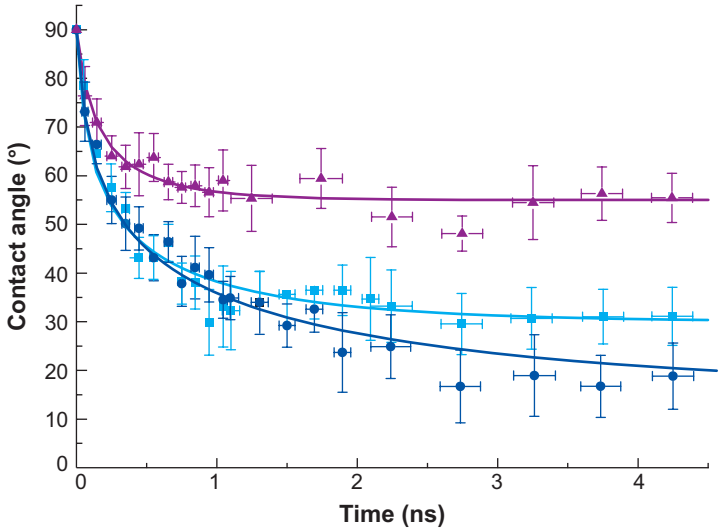

Figure 5

Evolution of the dynamic contact angle for simulations of capillary rise around a fiber for three solid-liquid interactions; from top to bottom $C_{SL} = D_{SL} = 0.9$, 1.0, and 1.05 (31).

able to calculate K^0. These results are also given in **Table 1** and show a corresponding decrease in frequency with increasing *S-L* interaction.

5.1.2. Wetting of fibers. When a fiber is put into contact with a liquid reservoir, provided that the equilibrium contact angle is less than 90°, the liquid will rise up spontaneously around the fiber. Seveno and coworkers (31, 53, 54) have studied the dynamics of this capillary rise both experimentally and in numerical simulation. **Figure 5** shows the evolution of the dynamic contact angle for three simulations with different solid-liquid interactions. The James equation (55) was used to calculate the contact angles from the meniscus profiles, assuming a quasi-static shape. The resulting behavior compares very well with experiment, as illustrated in **Figure 6** (54).

One can use Equation 2 to fit the data in **Figure 5** to obtain values of the contact-line friction (31). These values are shown in **Table 2**, expressed as the ratio γ/ζ^0. Because γ is constant, we again find that ζ^0 is a decreasing function of the equilibrium contact angle.

5.1.3. Imbibition. The imbibition of liquids into cylindrical pores has been studied over many years. In particular, it is known that the dynamics typically follow the Lucas-Washburn equation (56, 57),

$$x = \sqrt{\frac{\gamma R \cos\theta}{2\eta}}\sqrt{t}, \qquad 3.$$

where R is the radius of the pore. In the application of Equation 3, it is usually assumed that the contact angle is constant and equal to the equilibrium angle. For slow rates of penetration, this may not be an unreasonable assumption. In general, however, the angle will vary with the instantaneous velocity. Because the angle is difficult to measure experimentally, simulations offer an advantageous means of study. MD simulations carried out in this laboratory (30, 52) have shown good agreement with the Rideal-Washburn model if this is modified to account for the additional dissipation due to contact-line friction. **Figure 7** displays a typical snapshot of simulated capillary

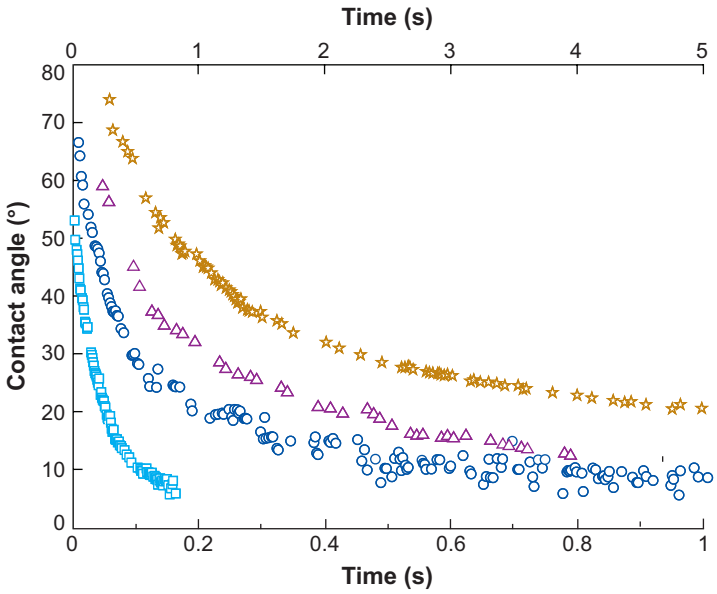

Figure 6

Evolution of the dynamic contact angle during capillary rise around a 0.8-mm-diameter poly(ethyleneterephthalate) fiber for four poly(dimethylsiloxanes) of different viscosity (54). From top to bottom: PDMS500 (timescale at *top*); PDMS50, PDMS20, and PDMS5 (timescale at *bottom*).

imbibition for a system containing approximately 145,000 liquid atoms in 16-atom chains. The understanding gained through this study enabled us to make some interesting predictions about the effect of the dynamic contact angle on the characterization of porous media (58), the influence of pore wettability on the speed of imbibition and drainage, and limitations imposed by dynamic wetting transitions (59).

5.2. Forced Spreading

In studies of forced spreading, the liquid is usually made to advance over the substrate at a set speed, which is then varied to study the influence of speed on dependent quantities such as the dynamic contact angle. This has obvious relevance to practical applications such as liquid coating. However, other examples of forced spreading include the initial stages of droplet impact and capillary imbibition driven by an external pressure.

5.2.1. Flat substrates. The pioneering simulations of Poiseuille and Couette flow by Koplik et al. (22, 23) and Thompson et al. (24, 25), respectively, are good examples of studies of the forced wetting of flat substrates. These researchers' model systems demonstrated macroscopic behavior that appeared consistent with experiment but also revealed microscopic details such as evidence

Table 2 Results obtained by applying a frictional dissipation model to the data of Figure 5 plus an additional data set for which $\theta^0 = 0$ (31)

$C_{SL} = D_{SL}$	0.9	1.0	1.05	1.25
θ^0 (°)	55.0	30.0	15.0	0
γ/ζ^0 (Å ns^{-1})	25.0	23.0	22.0	21.7

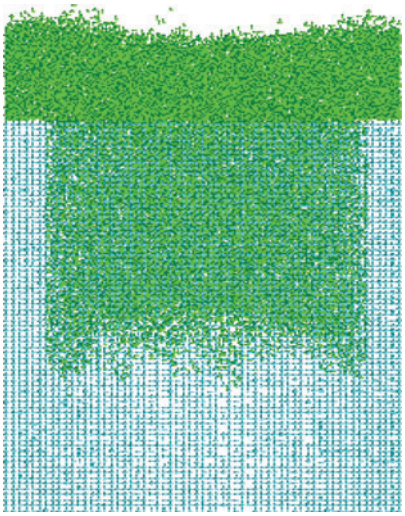

Figure 7

Snapshot of simulated capillary imbibition for a system containing approximately 145,000 liquid atoms in 16-atom chains, with $C_{SL} = D_{SL} = 1.0$ (30).

of molecular slip near the moving contact line. The studies involved two liquid phases. In our work (32), we have focused on large-scale simulations of a single, partially wetting liquid trapped between parallel flat plates, which are sheared in opposite directions (**Figure 8**). The system was extended in the direction parallel to the plates but perpendicular to the direction of shear by periodic boundary conditions. Two solid-liquid couplings were used, $C_{SL} = D_{SL} = 0.5$ and 0.8, yielding static contact angles of approximately 110° and 70°, respectively.

The system was first equilibrated until the contact angles converged and the shape of the liquid index became steady. After that, we began to move the plates by applying iterative shifts to their lattice positions at each time step, using appropriate periodic boundary conditions. We then

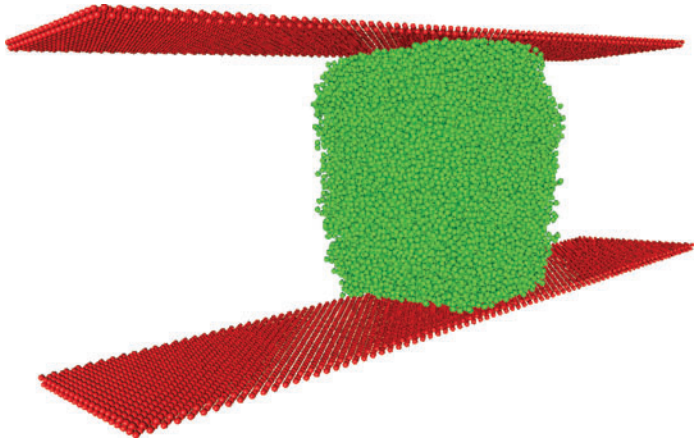

Figure 8

Perspective view of a partially wetting ($C_{SL} = D_{SL} = 0.5$) liquid index between two parallel plates at an early stage in the simulation (32). The index is composed of ~27,500 atoms in 16-atom chains.

observed the positions of the atoms within the index as a function of time. Contact angles were determined by methods similar to those for the spreading drops but were modified to account for the geometry of the system when under shear.

For the more wettable system, the receding dynamic contact angle fell rapidly with increasing speed, leading to rupture of the index. For the less wettable system, data could be obtained over a much greater range of speeds. Comparison with theory showed that all the data could be fitted with the MKT but that the low-speed data for the more wettable system were also consistent with the classical hydrodynamic theory of wetting, which predicts the so-called Tanner's law relationship: $v \sim \theta^3$ (60). This result illustrates the problem of establishing the validity of any theory when one is presented with a limited range of data (1).

5.2.2. Wetting of fibers. The forced wetting of a fiber has been studied over a range of solid-liquid interactions (33). A fiber of diameter 40 Å was centered within a liquid annulus composed of ~40,000 atoms in 16-atom chains. The outer rim of the annulus was frozen to maintain its geometry, leaving the upper and lower menisci to reach equilibrium. The fiber was constructed with 16,400 atoms arranged as a face-centered-cubic lattice. Periodic boundary conditions were applied longitudinally to simulate a fiber of infinite length. Once equilibrium had been established, the fiber was moved through the liquid at a constant speed, and the contact angle was measured with the James equation (54), a quasi-static interface, as before. Speeds from 0.02 m s^{-1} to 15 m s^{-1} were investigated. A typical side view of the process is shown in **Figure 9**. Results are plotted in **Figure 10** as $\cos\theta$ versus v for $C_{SL} = D_{SL} = 0.8$, 0.9, 1.0, and 1.05. Interestingly, the curves

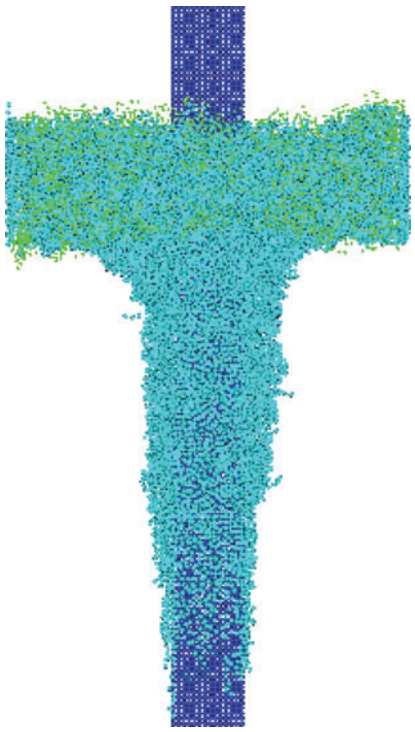

Figure 9

Side view of fiber wetting with $C_{SL} = D_{SL} = 0.8$ and a fiber velocity of 5 m s^{-1} (33).

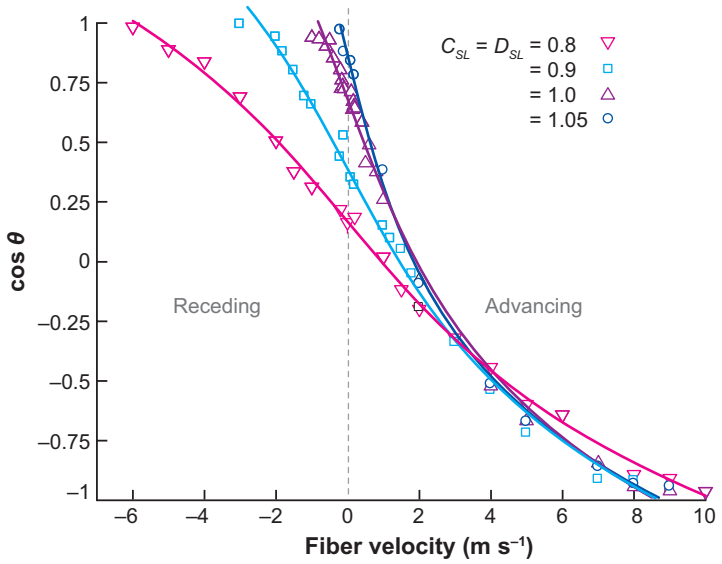

Figure 10

Cosine of the dynamic contact angle θ versus the fiber velocity for $C_{SL} = D_{SL} = 0.8$, 0.9, 1.0, and 1.05. The full lines are the best fits corresponding to the MKT (31).

converge at high wetting speeds, suggesting similar maximum speeds of wetting, independent of solid-liquid interaction over the range studied. The solid lines are the fits given by the MKT, showing rather good agreement. **Table 3** lists the resulting values of θ^0 and K^0. The conventional hydrodynamic theory is less successful in describing the data. As **Figure 11** demonstrates, the expected linear relationship is not obtained.

5.3. Mechanism of Wetting

As noted above, the fact that a simulation exhibits realistic macroscopic behavior is not sufficient to guarantee that the molecular mechanism is correct. Similarly, confirmation that a set of data can be fitted by a given theoretical equation is not sufficient to prove that the theory is correct. However, one of the advantages that MD has over experiment is that we can interrogate the detailed results at the molecular level and so verify whether the parameters obtained by applying a theoretical model actually match those of the system.

A key finding of many of the MD studies reviewed above is that the dynamic-contact-angle behavior closely follows that predicted by the MKT and is less well described by the standard hydrodynamic model. With simulations, as with physical experiments, the key variables λ, K^0,

Table 3 Frequency of displacements in the bulk liquid (f_{bulk}), within the first layer parallel to the solid ($f_{//}$), and between the first and second layer near the solid ($f_{\perp}$) as a function of solid-liquid interactions. All values are in reduced units

Solid-liquid interactions	f_{bulk}	$f_{//}$	$f_{\perp}$	K^0 (fit)
0.3	0.465	0.404	0.216	0.23
0.4	0.465	0.364	0.132	0.101
0.5	0.465	0.312	0.094	0.093

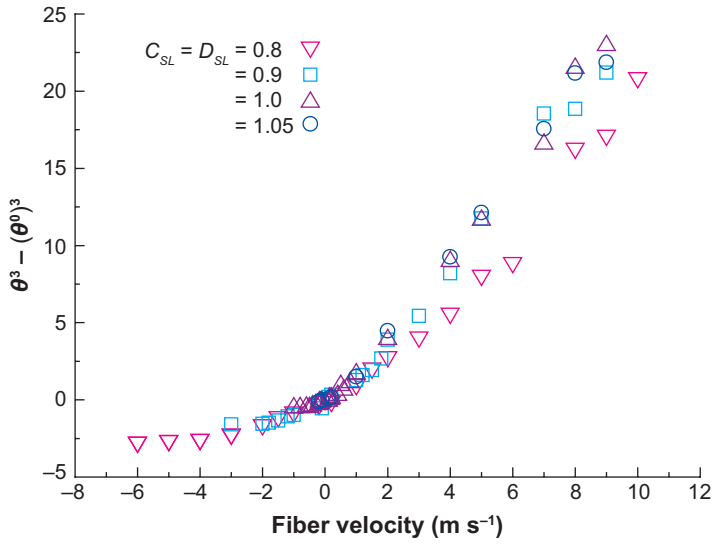

Figure 11

Fiber wetting data plotted in accordance with the standard hydrodynamic theory as $\theta^3 - (\theta^0)^3$ versus the fiber velocity for $C_{SL} = D_{SL} = 0.8$, 0.9, 1.0, and 1.05 (30).

and the friction ζ^0 can be obtained by fitting the data to the theoretical equations. However, with simulations, we can also measure the displacement frequency K^0 and the spacing λ directly from the simulations.

The natural choice of λ for the long-chain molecules in the simulations is the average interatomic distance. In the bulk, away from any interface, and at equilibrium, we may expect the displacement frequency to be isotropic. In the simulations of sessile drop spreading (26), for instance, we can measure the time it takes an atom to travel unit distance away from its initial position, at equilibrium. In **Figure 12**, the relative number of atoms that have already traveled unit distance is given as a function of the time.

We can divide this curve in three parts. For a short initial time, no atoms are counted. This is the time that even the fastest atoms require to move a unit distance. This region is followed by one with a sharp rise. At longer times, the curve slowly approaches 100%, indicating that some

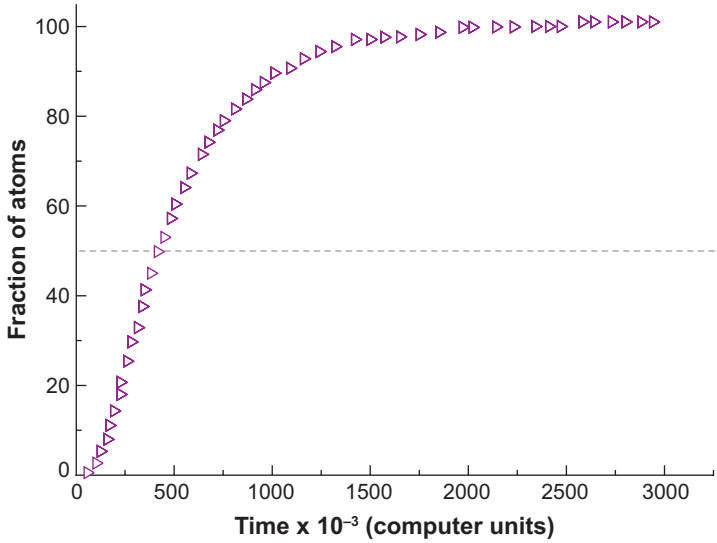

Figure 12

Percentage of atoms in the bulk that have moved unit distance away from their initial position as a function of the elapsed time (26). The dashed line is at 50%.

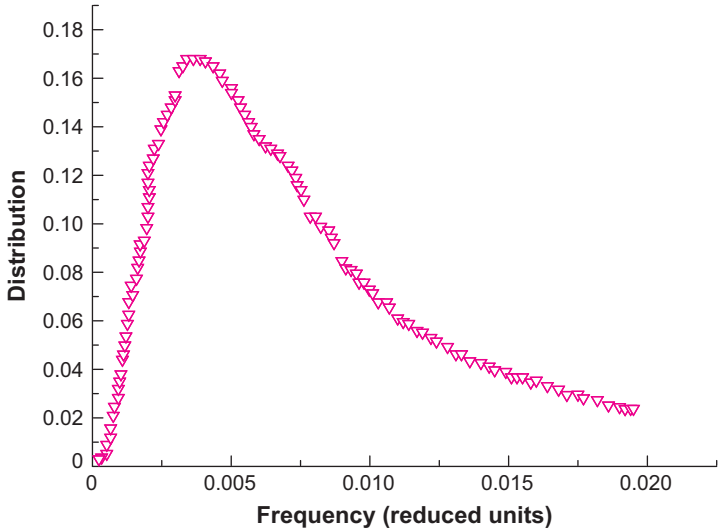

Figure 13

The frequency distribution of atoms in the bulk of the drop, associated with $\lambda = 1.0$ r.u., at equilibrium.

atoms stay close to their initial positions for a long time. By differentiating and inverting these measurements, we obtain the frequency distribution in the bulk associated with $\lambda = 1.0$ r.u. This is plotted in **Figure 13**. Evidently, the distribution is not exactly Gaussian.

Most of the macroscopic characteristics of liquids are the result of the collective action of many atoms acting together. This is certainly true for wetting. Thus, it is not necessary to consider the complete distribution of frequencies in **Figure 13**. Instead, we can characterize the molecular behavior in terms of the average time t_{bulk}. This time is easy to determine from **Figure 12**: It is the time at which half of the atoms have traveled unit distance. The average frequency f_{bulk} is then the inverse of this time. For the bulk atoms at equilibrium, this average frequency is 2.32×10^{-3} in computer units or 0.465 r.u. (26).

Near the solid, however, we may expect the displacement frequencies to be anisotropic. Evidence of this comes from the layering that occurs near attractive walls and that is also seen in simulations (46). Layers clearly indicate long residence times within a given layer and, therefore, relatively slow diffusion between them. For molecules in contact with the solid, one can distinguish two frequencies, namely, those from displacements parallel to the solid surface $f_{//}$ (i.e., displacement within the same liquid layer) and those perpendicular to the solid surface $f_{\perp}$ (i.e., displacement from one layer to another). To compute these frequencies, the density profile must first be computed to locate the liquid layers.

Because the number density within each layer is approximately the same as within the bulk, we can assume the same unit distance. In **Figure 14**, the cumulative number of atoms that have moved unit distance within the first layer is given as a function of elapsed time and solid-liquid interaction. As before, we determine the average frequency as the inverse of the time required for displacement of 50% of the atoms. The calculated values, given in **Table 3**, reveal that the time required for half the number of atoms to travel unit distance in the first layer depends on the solid-liquid interaction potential and is always larger than in the bulk.

In the frequency domain, this means that $f_{//}$ is lower than f_{bulk}; i.e., the atoms in the bulk are more free to move and the associated velocities are higher than those in the first layer near the

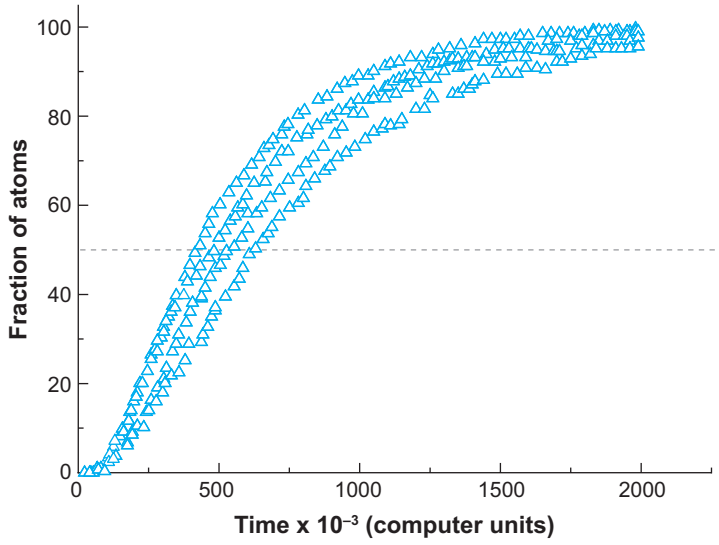

Figure 14

Percentage of atoms in the first layer that have moved unit distance away from their initial position as a function of elapsed time and solid-liquid interactions (26). The curve for the bulk from **Figure 12** is shown as a reference. From left to right: bulk, $C_{sf} = D_{sf} = 0.3$, $C_{sf} = D_{sf} = 0.4$, and $C_{sf} = D_{sf} = 0.5$. The dashed line is at 50%.

solid. Furthermore, as the solid-liquid interaction is increased, $f_{//}$ within the first layer decreases; i.e., the atoms are more strongly bound to the solid and are less easily displaced. In other words, the mobility parallel to the solid is increasingly restricted with increasing solid-liquid interactions. This result is key to our understanding of the dissipative processes occurring within the TPZ during wetting.

We can follow the same procedure to calculate the frequency of displacements between the first and the second layers next to the solid $f_{\perp}$. The distance between the centers of these layers turns out to be 0.8 r.u., so this is taken as the unit distance. **Figure 15** shows the cumulative percentage of atoms that have moved between the first and second layers as a function of elapsed time and solid-liquid interactions. The same trend is evident here as for $f_{//}$; however, the effect is much more pronounced. Displacement times are roughly doubled compared with those in the bulk, even for the weakest solid-liquid interactions ($C_{sf} = D_{sf} = 0.3$), and increase steeply with coupling.

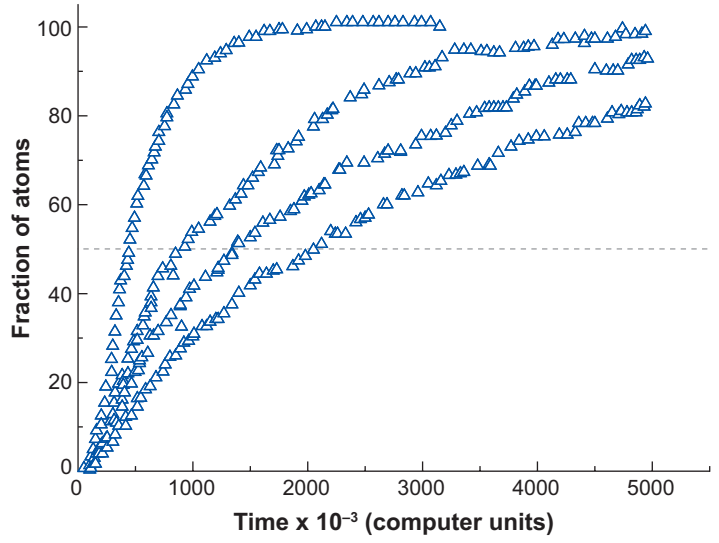

Figure 15

Percentage of atoms that have moved between the first and second layers as a function of elapsed time and solid-liquid interactions (26). The curve for the bulk from **Figure 12** is shown as a reference. From left to right: bulk, $C_{sf} = D_{sf} = 0.3$, $C_{sf} = D_{sf} = 0.4$, and $C_{sf} = D_{sf} = 0.5$. The dashed line is at 50%.

Thus, consistent with the observed layering near the solid, displacements normal to the interface are retarded more strongly than displacements along the surface, and mobility is therefore highly anisotropic, as anticipated. **Table 3** lists the calculated values of $f_\perp$.

All the frequencies discussed above are equilibrium characteristics. Application of a potential gradient, i.e., a force, is required to produce a net flow. This is also the case at the contact line and forms the basis of the MKT. That f_{bulk} is greater than both $f_{//}$ and $f_\perp$ explains the origin of contact-line friction: A larger force will be required for a given rate of flow. Furthermore, as wetting proceeds and solid-liquid contact area increases, atoms from the second layer will be required to repopulate the first. Because $f_{//} > f_\perp$, repopulation is evidently the slower process. It will therefore be the rate-limiting step and the one most likely to determine K^0. Thus, we can compare these direct measurements with the values of K^0 obtained by fitting the dynamic-contact-angle data to the MKT. This comparison is shown in the final column of **Table 3**. The good agreement between K^0 and $f_\perp$ strongly suggests not only that we have correctly identified the mechanism of wetting but that the MKT provides an accurate description of dynamic wetting process in these simulated systems. Similar agreement has also been found for the simulated wetting of fibers (33, 53).

5.4. Predictive Tools

Once the simulation model has been validated, it can be used to investigate effects that are difficult to study experimentally. It also enables us to use the computer simulations as predictive tools. One of the important spin-offs from our studies is the confirmation that K^0 and ζ^0 are simple functions of the energy of adhesion between the liquid and the solid. According to a recent development of the MKT, $\zeta^0 \sim \eta \exp(\gamma(1+\cos\theta^0)\lambda^2/k_BT)$, where $\gamma(1+\cos\theta^0)$ is the work of adhesion. This relationship between the friction ζ^0 and the work of adhesion is tested in **Figure 16** by plotting $-\ln(\zeta^0/\gamma)$ versus $(1+\cos\theta^0)$ with data from the simulations of capillary rise around a fiber (**Table 2**) (31). Both the surface tension and viscosity are constant for these simulations, so a straight line of negative slope is predicted and indeed observed. As discussed by Blake & De Coninck (11), this result means that the dynamics of wetting tends to be slower on well-wetted

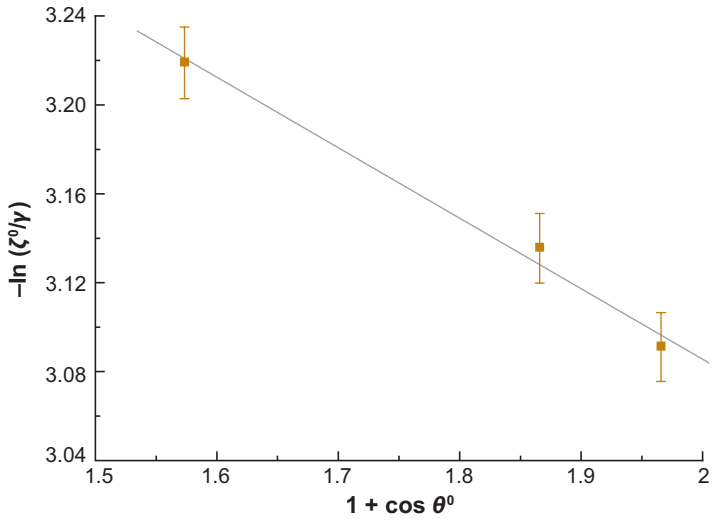

Figure 16

Plot of $-\ln(\zeta^0/\gamma)$ versus $(1+\cos\theta^0)$ for data from simulations of capillary rise around a fiber (31).

surfaces and leads to nonmonotonous behavior of the maximum speed of wetting versus the equilibrium contact angle.

6. CONCLUSIONS

In this chapter, we show that large-scale MD simulations can be used to study wetting in many situations. We use a very simple model of linear liquid molecules and an atomic solid, with the atoms of a given molecule connected by a strong harmonic potential and intermolecular interactions of the Lennard-Jones type. Upon changing the strength of the solid-liquid interaction, we can vary the wettability from very nonwettable to complete wetting. One of the important benefits of the simulations is that we are able to measure, simultaneously, both macroscopic and microscopic characteristics of the dynamic wetting. Thus, we can measure, on the one hand, surface tension, viscosity, and the contact angle and, on the other hand, the relevant molecular quantities such as the molecular displacement frequencies. Although different existing models can be used to fit the dynamic-contact-angle data by the use of various fitting parameters, we demonstrate that the description of dissipation on the microscopic scale, as proposed in the MKT, seems to be correct—at least for these simulated systems. By extracting the details of the molecular processes occurring in the simulations, we also show that the physical interpretation of the parameters is fully consistent with the model. We believe that this is a key step in validating any simulation. Improving models and increasing computer power may one day mean that simulations of wetting will take precedence over experiment. However, in developing our models it is important that we take all necessary steps to ensure that they not only reflect the physical world with accuracy but also have internal integrity.

SUMMARY POINTS

1. Large-scale molecular dynamics (MD) is an effective way to study the dynamics of both spontaneous and forced wetting in a wide range of geometries.
2. Simple Lennard-Jones potentials are used but are combined with additional potentials to replicate intramolecular bonds and ensure solid integrity.
3. Static and dynamic contact angles are measured in ways that mimic macroscopic methods. Colligative properties such as surface tension and viscosity can be obtained by standard statistical mechanics.
4. Current simulations can accommodate of the order of 10^6 liquid atoms. Although this is still relatively small compared with real physical systems, it is sufficient to investigate behavior at both the global macroscopic level as well as the molecular level, normally inaccessible to experiments.
5. MD provides opportunities to vary the properties of the interacting media in ways that are not readily possible in experiments. For example, one can change the solid-liquid interaction without changing any other properties of the liquid or solid.
6. The results of simulations provide insight into the underlying mechanisms by which contact lines can advance across a solid surface. Studies in our lab and others' suggest that the molecular-kinetic theory (MKT) provides an effective description of this process in terms of the length λ and the equilibrium frequency K^0 of molecular displacements.

7. The ability to fit experimental or simulation data by the use of a theoretical relationship is not sufficient to prove the underlying validity of the theory. However, with simulations it is possible to analyze the detailed molecular activity to check for internal consistency. When this is done, we obtain good agreement between the values of K^0 and λ obtained from the fits and directly from the simulations. This internal check provides strong evidence to support the MKT for these simulated systems.

1. A critical review of theories of dynamic wetting and their comparison with experiment.

2. Applied the lubrication model to dynamic wetting. Showed that the no-slip condition leads to a divergent stress field at the moving contact line.

3. Lubrication model of dynamic wetting giving an explicit expression for the velocity dependence of the dynamic contact angle ($\theta \sim v^{1/3}$).

6. Hydrodynamic model of dynamic wetting that includes interfacial transformation.

8. Frenkel-Eyring theory of fluid transport as a stress-modified molecular rate process applied to dynamic wetting. Derived explicit expressions for the velocity dependence of the contact angle.

10. Reviewed the molecular-kinetic theory of dynamic wetting. Added the effect of liquid viscosity to the model.

DISCLOSURE STATEMENT

The authors are not aware of any biases that might be perceived as affecting the objectivity of this review.

ACKNOWLEDGMENTS

The authors thank the partial financial support of the Fonds National pour la Recherche Scientifique and the Région Wallone.

LITERATURE CITED

1. **Blake TD. 2006. The physics of moving wetting lines. *J. Colloid Interface Sci.* 299:1–13**
2. **Huh C, Scriven LE. 1971. Hydrodynamic model of steady movement of a solid/liquid/fluid contact line. *J. Colloid Interface Sci.* 35:85–101**
3. **Voinov OV. 1976. Hydrodynamics of wetting. *Fluid Dyn.* 11:714–12**
4. Cox RG. 1986. The dynamics of the spreading of liquids on a solid surface. *J. Fluid Mech.* 168:169–94
5. Ngan CG, Dussan V. EB. 1989. On the dynamics of liquid spreading on solid surfaces. *J. Fluid Mech.* 209:191–226
6. **Shikhmurzaev YD. 1997. Moving contact lines in liquid/liquid/solid systems. *J. Fluid Mech.* 334:211–49**
7. Cherry BW, Holmes CM. 1969. The kinetics of the wetting of surfaces by polymers. *J. Colloid Interface Sci.* 29:174–76
8. **Blake TD, Haynes JM. 1969. Kinetics of liquid/liquid displacement. *J. Colloid Interface Sci.* 30:421–23**
9. Ruckenstein E, Dunn CS. 1977. Slip velocity during wetting of solids. *J. Colloid Interface Sci.* 59:135–38
10. **Blake TD. 1993. Dynamic contact angles and wetting kinetics. In *Wettability*, ed. JC Berg, pp. 251–309. New York: Dekker**
11. Blake TD, De Coninck J. 2002. The influence of solid-liquid interactions on dynamic wetting. *Adv. Colloid Interface Sci.* 96:21–36
12. Voué M, De Coninck J. 2000. Spreading and wetting at the microscopic scale: recent developments and perspectives. *Acta Mater.* 48:4405–417
13. Metropolis N, Rosenbluth AW, Rosenbluth MN, Teller AH, Teller E. 1953. Equation of state calculations by fast computing machines. *J. Chem. Phys.* 21:1087–92
14. Alder BJ, Wainwright TE. 1957. Phase transition for a hard sphere system. *J. Chem. Phys.* 27:1208–9
15. Rahman A. 1964. Correlations in the motion of atoms in liquid argon. *Phys. Rev.* 136A:405–11
16. Saville G. 1977. Computer simulation of the liquid-solid-vapour contact angle. *Faraday II* 73:1122–32
17. Allen MP, Tildesley DJ. 1987. *Computer Simulations of Liquids*. Oxford, UK: Oxford Univ. Press
18. De Coninck J, Hoorelbeke S, Valignat MP, Cazabat A-M. 1993. Effective microscopic model for the dynamics of spreading. *Phys. Rev. E* 48:4549–55
19. De Coninck J, D'Ortona U, Koplik J, Banavar JR. 1995. Terraced spreading of chain molecules via molecular dynamics. *Phys. Rev. Lett.* 74:928–31

20. D'Ortona U, De Coninck J, Koplik J, Banavar JR. 1996. Terraced spreading mechanisms for chain molecules. *Phys. Rev. E* 53:562–69
21. De Coninck J, Voué M. 1997. The dynamics of spreading at the microscopic scale. *Interface Sci.* 5:141–45
22. **Koplik J, Banavar JR, Willemsen JF. 1988. Molecular dynamics of Poiseuille flow and moving contact lines. *Phys. Rev. Lett.* 60:1282–85**
23. Koplik J, Banavar JR, Willemsen JF. 1989. Molecular dynamics of fluid flow at solid surfaces. *Phys. Fluids A* 1:781–94
24. Thompson PA, Brinckerhoff WB, Robbins MO. 1993. Microscopic studies of static and dynamic contact angles. *J. Adhes. Sci. Technol.* 7:535–41
25. **Thompson PA, Robbins MO. 1989. Simulations of contact-line motion: slip and the dynamic contact angle. *Phys Rev. Lett.* 63:766–69**
26. **De Ruijter MJ, Blake TD, De Coninck J. 1999. Dynamic wetting studied by molecular modeling simulations of droplet spreading. *Langmuir* 15:7836–47**
27. Blake TD, Decamps C, De Coninck J, de Ruijter M, Voué M. 1999. The dynamics of spreading at the microscopic scale. *Colloids Surf.* 154:5–11
28. Heine DR, Grest GS, Webb EB III. 2003. Spreading dynamics of polymer nanodroplets. *Phys. Rev. E* 68:061603
29. Heine DR, Grest GS, Webb EB III. 2004. Spreading dynamics of polymer nanodroplets in cylindrical geometries. *Phys. Rev. E* 70:011606
30. Martic G, Gentner F, Seveno D, Coulon D, De Coninck J, Blake TD. 2002. A molecular dynamics simulation of capillary imbibition. *Langmuir* 18:7971–76
31. Seveno D, De Coninck J. 2004. Possibility of different time scales in the capillary rise around a fiber. *Langmuir* 20:737–42
32. **Gentner F, Ogonowski G, De Coninck J. 2003. Forced wetting dynamics: a molecular dynamics study. *Langmuir* 19:3996–4003**
33. **Seveno D, Ogonowski G, De Coninck J. 2004. Liquid coating of moving fiber at the nanoscale. *Langmuir* 20:8385–90**
34. Adão MH, de Ruijter M, Voué M, De Coninck J. 1999. Droplet spreading on heterogeneous substrates using molecular dynamics. *J. Phys. Rev. E* 59:746–50
35. Martic G, Blake TD, De Coninck J. 2005. Dynamics of imbibition into a pore with a heterogeneous surface. *Langmuir* 21:11201–7
36. Grest G, Heine DR, Webb EB III. 2006. Liquid nanodroplets spreading on chemically patterned surfaces. *Langmuir* 22:4745–49
37. Seveno D, Ledauphin V, Martic G, Voué M, De Coninck J. 2002. Spreading drop dynamics on porous surfaces. *Langmuir* 18:7496–502
38. Bertrand E, Blake TD, De Coninck J. 2005. Spreading dynamics of chain-like monolayers: a molecular dynamics study. *Langmuir* 21:6628–35
39. Supple S, Quirke N. 2004. Molecular dynamics of transient oil flows in nanopores 1: imbibition speeds for single wall carbon nanotubes. *J. Chem. Phys.* 121:6571–79
40. Swiler TP, Loehman RE. 2000. Molecular dynamics simulations of reactive wetting in metal-ceramic systems. *Acta Mater.* 48:4419–24
41. Webb EB III, Grest GS, Heine DR. 2003. Precursor film controlled wetting of Pb on Cu. *Phys. Rev. Lett.* 91:236102
42. Webb EB III, Grest GS, Heine DR, Hoyt JJ. 2005. Dissolutive wetting of Ag on Cu: a molecular dynamics simulation study. *Acta Mater.* 53:3163–77
43. Berttrand E, Blake TD, Ledauphin G, Ogonowski G, De Coninck J. 2007. Dynamics of dewetting at the nanoscale using molecular dynamics. *Langmuir* 23:3774–85
44. Press WH, Teukolsky SA, Vetterling WT, Flannery BP. 1992. *Numerical Recipes in Fortran*. Cambridge, UK: Cambridge Univ. Press. 2nd ed.
45. Blake TD, Clarke A, De Coninck J, de Ruijter MJ. 1997. Contact angle relaxation during droplet spreading: comparison between molecular kinetic theory and molecular. *Langmuir* 13:2164–66
46. Galea TM, Attard P. 2004. Molecular dynamics study of the effect of atomistic roughness on the slip length at the fluid-solid boundary during shear flow. *Langmuir* 20:3477–82

22. The pioneering application of molecular dynamics to dynamic wetting in Poiseuille flow.

25. The pioneering application of molecular dynamics to dynamic wetting in Couette flow.

26. Large-scale application of molecular dynamics. Studied the influence of solid-liquid interactions and showed agreement between molecular-kinetic theory and simulations.

32. A molecular dynamics study of the forced wetting on flat substrates, showing velocity dependence of the contact angle and the flow field in the vicinity of the solid surface.

33. A molecular dynamics study of the forced wetting of fibers, showing velocity dependence of the contact angle and the flow field around the fiber.

47. Priezjev NV, Darhuber AA, Troian SM. 2005. Slip behavior in liquid films on surfaces of patterned wettability: comparison between continuum and molecular dynamics simulations. *Phys. Rev. E* 71:041608
48. Voronov RS, Papavassiliou DV, Lee LL. 2006. Boundary slip and wetting properties of interfaces: correlation of the contact angle with slip length. *J. Chem. Phys.* 124:204701–10
49. Hoover WG. 1985. Canonical dynamics: equilibrium phase-space distributions. *Phys. Rev. A* 31:1695–97
50. Nosé S, Yonezawa F. 1986. Isothermal–isobaric computer simulations of melting and crystallization of a Lennard-Jones system. *J. Chem. Phys.* 84:1803–14
51. de Ruijter MJ, De Coninck J, Blake TD, Clarke A, Rankin A. 1997. Contact angle relaxation during the spreading of partially wetting drops. *Langmuir* 13:7293–98
52. Martic G, Gentner F, Seveno D, De Coninck J, Blake TD. 2004. The possibility of different time scales in the dynamics of pore imbibition. *Colloid Interface Sci.* 270:171–79

52a. Rowlinson JS, Widom B. 1989. *Molecular Theory of Capillarity*. Oxford, UK: Clarendon

53. Seveno D. 2004. *Dynamic wetting of fibers*. PhD thesis. Fac. Polytech. Mons, Belg. 100 pp.
54. Vega M-J, Seveno D, Lemaur G, Adão M-H, De Coninck J. 2005. Dynamics of the rise around a fiber: experimental evidence of the existence of several time scales. *Langmuir* 21:9584–90
55. James DF. 1974. The meniscus on the outside of a small circular cylinder. *J. Fluid Mech.* 63:657–64
56. Lucas R. 1918. Ueber das Zeitgesetz des Kapillaren Aufstiegs von Fluussigkeiten. *Kolloid Z.* 23:15–22
57. Washburn EW. 1921. The dynamics of capillary flow. *Phys. Rev.* 17:273–83
58. Martic M, De Coninck J, Blake TD. 2003. Influence of the dynamic contact angle on the characterisation of porous media. *J. Colloid Interface Sci.* 263:213–16
59. Blake TD, De Coninck J. 2004. The influence of pore wettability on the dynamics of imbibition and drainage. *Colloids Surf. A* 250:395–402
60. Tanner LH. 1979. The spreading of silicone oil drops on horizontal surfaces. *J. Phys. D* 2:1473–84